Journal of Materials Chemistry A

Accepted Manuscript

ROYAL SOCIETY OF CHEMISTRY

www.rsc.org/materialsA

Journal Name

ARTICLE

Silver-Inserted Zinc Rhodium Oxide and Bismuth Vanadium Oxide Heterojunction Photocatalyst for Overall Pure-Water Splitting under Red Light

Received 00th January 20xx,
Accepted 00th January 20xx

DOI: 10.1039/x0xx00000x

www.rsc.org/

Ryoya Kobayashi,[a] Kazuki Kurihara,[b] Toshihiro Takashima,[c] Bunsho Ohtani[d] and Hiroshi Irie*[c]

We have prepared a solid-state heterojunction photocatalyst, in which zinc rhodium oxide ($ZnRh_2O_4$) and bismuth vanadium oxide ($Bi_4V_2O_{11}$) as hydrogen (H_2) and oxygen (O_2) evolution photocatalysts, respectively, were connected with silver (Ag, $ZnRh_2O_4$/Ag/$Bi_4V_2O_{11}$). $ZnRh_2O_4$/Ag/$Bi_4V_2O_{11}$ was able to photocatalyze overall pure-water splitting under red-light irradiation with a wavelength of 700 nm. On the basis of the analogy with a solid-state heterojunction photocatalyst composed of $ZnRh_2O_4$, defective silver antimonate ($Ag_{1-x}SbO_{3-y}$), and Ag (R. Kobayashi *et al.*, *J. Phys. Chem. C*, 2014, 118, 22450-22456), we consider that the overall water-splitting performance of the $ZnRh_2O_4$/Ag/$Bi_4V_2O_{11}$ photocatalyst was derived from the photoproduced holes that were generated in the valence band (VB) of $Bi_4V_2O_{11}$ contributing to O_2 liberation and the photoexcited electrons that were generated in the conduction band (CB) of $ZnRh_2O_4$ contributing to H_2 liberation. Importantly, Ag possibly acts as a solid-state electron mediator for the transfer of electrons from the CB of $Bi_4V_2O_{11}$ to the VB of $ZnRh_2O_4$.

Introduction

Since Fujishima and Honda reported photoelectrochemical water splitting using a TiO_2 electrode in 1972,[1] solar hydrogen (H_2) production from water using a semiconductor photocatalyst has attracted attention as a clean energy resource. In terms of simplicity and the possibility of large-scale H_2 production, water splitting by powdered photocatalysts is currently a subject of considerable interest. In fact, numerous studies have attempted to identify powdered photocatalysts that are able to split water into H_2 and oxygen (O_2) at a molar ratio of ~2 : 1 (overall water splitting),[2-26] particularly under visible-light irradiation for the efficient utilization of incoming sunlight.[8-26] One of the major approaches to visible-light sensitization is to construct a system composed of a single photocatalyst whose electric band structure is controlled and a suitable cocatalyst,[8-16] the most well-known example being the gallium nitride (GaN) –zinc oxide (ZnO) solid solution reported by Domen and coworkers.[8-11] Recently, quite a few photocatalysts have been developed,[12-19] and among them nanocrystalline CoO can be sensitive to visible light without the use of a cocatalyst.[17] Very recently, Pan *et al.* reported a Rh–Cr oxide ($RhCrO_y$)-loaded lanthanum–magnesium–tantalum oxynitride ($LaMg_xTa_{1-x}O_{1+3x}N_{2-3x}$) solid solution with a bandgap (Eg) of 2.03 eV loaded with titanium and silicon amorphous oxyhydroxides ($MO_{2-m}(OH)_{2m}\cdot xH_2O$) as coating layers.[18] According to the authors, this complex photocatalyst is operable up to a wavelength of 600 nm. Liu *et al*. reported a carbon nanodot–carbon nitride (C_3N_4) nanocomposite as a metal-free photocatalyst, and demonstrated its performance for overall water splitting when irradiated with visible light with a wavelength of 630±20 nm, which is the longest reported wavelength for overall water splitting.[19]

Another approach is to construct a system composed of double photocatalysts sensitive to visible light, called the "Z-scheme", which was first reported by Sayama and coworkers, who used platinum (Pt)-deposited chromium-and-tantalum-codoped strontium titanate (Pt/$SrTiO_3$:Cr,Ta) as a H_2 evolution photocatalyst (H_2 photocatalyst) and Pt-deposited tungsten trioxide (Pt/WO_3) as an O_2 evolution photocatalyst (O_2 photocatalyst).[20] After that, numerous Z-scheme systems were reported in which various H_2 and O_2 photocatalysts were combined.[21-23] Most of these systems must employ a suitable redox mediator such as iodate ions (IO_3^-)/iodide ions (I^-) or ferric ions (Fe^{3+})/ferrous ions (Fe^{2+}). However, all the previously reported Z-scheme systems are only able to utilize visible light up to a wavelength of 520 nm. In addition, such conventional Z-scheme systems require a redox mediator, meaning that they are not capable of splitting "pure" water (i.e., distilled water with no added chemicals). Recently, solid-state

[a] *Special Doctoral Program for Green Energy Conversion Science and Technology, Interdisciplinary Graduate School of Medicine and Engineering, University of Yamanashi, 4-3-11 Takeda, Kofu, Yamanashi 400-8511, Japan*
[b] *Department of Applied Chemistry, Interdisciplinary Graduate School of Medicine and Engineering, University of Yamanashi, 4-3-11 Takeda, Kofu, Yamanashi 400-8511, Japan*
[c] *Clean Energy Research Center, University of Yamanashi, 4-3-11 Takeda, Kofu, Yamanashi 400-8511, Japan*
[d] *Catalysis Research Center, Hokkaido University, Nishi 10, Kita 21, Sapporo 001-0021, Japan*

Electronic Supplementary Information (ESI) available: [details of any supplementary information available should be included here]. See DOI: 10.1039/x0xx00000x

Z-scheme systems that function in the absence of a redox mediator have been reported. However, it was necessary to adjust the pH to 3.5 using sulfuric acid (H_2SO_4),[24,25] so in this sense, pure-water splitting was not accomplished.

Recently, we have developed a novel solid-state photocatalyst by inserting silver (Ag) as an electron mediator between zinc rhodium oxide ($ZnRh_2O_4$, Eg of 1.2 eV) and defective silver antimonite ($Ag_{1-x}SbO_{3-y}$, Eg of 2.7 eV) as H_2 and O_2 photocatalysts, respectively ($ZnRh_2O_4$/Ag/$Ag_{1-x}SbO_{3-y}$).[26] In this system, we achieved overall pure-water splitting catalyzed via the inserted Ag, which could transfer photoexcited electrons from the conduction band (CB) of $Ag_{1-x}SbO_{3-y}$ to the valence band (VB) of $ZnRh_2O_4$. The $ZnRh_2O_4$/Ag/$Ag_{1-x}SbO_{3-y}$ utilized visible light up to a wavelength of 545 nm depending on the photoabsorption capability of the $Ag_{1-x}SbO_{3-y}$. Therefore, to improve the photosensitivity of this system at longer wavelengths of light, we searched for a new, smaller-bandgap O_2 photocatalyst to replace $Ag_{1-x}SbO_{3-y}$, and we found that bismuth vanadium oxide ($Bi_4V_2O_{11}$), which has an Eg of 1.6–2.2 eV, is a promising material.[27]

In the present study, we attempted to construct an Ag-inserted heterojunction system ($ZnRh_2O_4$/Ag/ $Bi_4V_2O_{11}$) using our reported method,[26] and we demonstrated that this system can accomplish overall pure-water splitting under visible light up to 700 nm (red light), which we believe is the longest wavelength reported so far.

Experimental

Sample preparation

$ZnRh_2O_4$ and $Bi_4V_2O_{11}$ powders were synthesized using a solid-state reaction method. Commercial zinc oxide (ZnO, Kanto Kagaku, purity 99.0%) and rhodium oxide (Rh_2O_3, Kanto Kagaku, purity 99.9%) powders were used for $ZnRh_2O_4$, and bismuth oxide (Bi_2O_3, Kanto Kagaku, purity 99.9%) and vanadium oxide (V_2O_5, Kanto Kagaku, purity 99.0%) powders were used for $Bi_4V_2O_{11}$ as the starting materials. Stoichiometric amounts of the starting materials for both materials were wet-ball-milled for 20 h in polyethylene bottles using zirconium dioxide (ZrO_2) balls as the milling medium. The resulting mixtures were calcined at 1000°C for 24 h and 850°C for 8 h to obtain $ZnRh_2O_4$ and $Bi_4V_2O_{11}$ powders, respectively. Then, the obtained powders were thoroughly ground.

A powdered photocatalyst heterojunction composed of $ZnRh_2O_4$ and $Bi_4V_2O_{11}$ with Ag between them ($ZnRh_2O_4$/Ag/$Bi_4V_2O_{11}$) was prepared using the following straightforward method. $Bi_4V_2O_{11}$, Ag_2O, and $ZnRh_2O_4$ powders with a molar ratio of 1:1:1 were wet-ball-milled in an identical manner to above. The mixed powders were pressed into pellets by applying a force of 60 kN, and then the pellets were heated at 750°C for 2 h. After grinding the pellets into a fine powder, the powder was soaked in nitric acid (HNO_3, Kanto Kagaku) aqueous solution (3 M, 50 mL) for 30 min. The powder was subsequently filtered then washed with a sufficient amount of distilled water and dried at 65°C for 12 h.

Characterization

The crystal structures of the prepared powders were determined by X-ray diffraction (XRD) (PW-1700, PANalytical). The Ag 3d core levels were measured by X-ray photoelectron spectroscopy (XPS; AXIS ULTRA, Shimadzu) to confirm the valency of Ag. UV-visible absorption (UV-vis) spectra were obtained by the diffuse reflection method using a spectrometer (V-650, JASCO) with barium sulfate ($BaSO_4$) as the reflectance standard. A scanning electron microscope (SEM, JSM-6500F, JEOL) was used to observe the morphology of the prepared photocatalysts. A scanning transmission electron microscope (STEM, Tecnai Osiris, FEI) was also utilized with element maps obtained by energy-dispersive X-ray spectrometry (EDS).

Water-splitting reactions

The following photocatalytic O_2 evolution reaction and overall water splitting tests were conducted in a gas-closed circulation system. Argon gas (50 kPa) was introduced into the system after repeated deaeration down to 2.5 Pa. The amounts of evolved H_2 and O_2 were monitored using an online gas chromatograph (GC-8A, Shimadzu).

$Bi_4V_2O_{11}$ powder (60 mg) with either silver nitrate ($AgNO_3$; Kanto Kagaku, 0.1 mol/L) or cerium sulfide ($Ce(SO_4)_2$, Kanto Kagaku, 0.1 mol/L) as a sacrificial agent was suspended in 12 mL water without adjusting the pH of the solution and stirred using a magnetic stirrer (Fig. S1 in ESI. 1). Light-emitting diode (LED) lamps with wavelengths of 610 and 700 nm (hereafter, 610 nm LED and 700 nm LED, LEDH60-610 and LEDH60-700, respectively, Hamamatsu Photonics) were employed to confirm the evolution of O_2. The apparent quantum efficiency (AQE) for each wavelength was then evaluated. The AQE values for O_2 evolution were calculated using the equation AQE (%) = 100 × 4 × O_2 evolution rate/incident photon rate because the O_2 evolution is represented by the formula $2H_2O + 4h^+ \rightarrow O_2 + 4H^+$.

The $ZnRh_2O_4$/Ag/$Bi_4V_2O_{11}$ composite powder (60 mg) was suspended in 12 mL pure water (without adjusting the pH of the water) and stirred using a magnetic stirrer. A xenon (Xe) lamp (LA-251Xe, Hayashi Tokei) with an optical filter (Y-44, Hoya, irradiated wavelength > 420 nm), the 610 nm LED, and the 700 nm LED were used for light irradiation. AQE values were calculated using the amount of evolved O_2 in the same way as described above.

To scale up the overall water-splitting reaction, 600 mg of the composite powder was suspended in 120 mL pure water (without adjusting the pH of the water) and stirred using a magnetic stirrer. Accordingly, the reaction vessel was changed from one with a volume of ~10 cm^3 to one with a volume of ~250 cm^3. In this case, two Xe lamps with Y-44 optical filters were used for light irradiation of the powder.

A photocatalytic overall water-splitting test was also conducted in a gas-closed circulation system connected to a gas chromatograph mass spectrometer (GCMS, GCMS-QP 2010 Ultra, Shimadzu) using pure water containing 33% isotopic water ($H_2{}^{18}O$, Aldrich Chemistry, purity 97 atm% ^{18}O) under light irradiation emitted from the 700 nm LED. The evolved gas was detected by the GCMS, which was operated in the selective-ion mode and monitored ions with masses of 28 ($^{14}N^{14}N$), 32 ($^{16}O^{16}O$), 34 ($^{18}O^{16}O$), and 36($^{18}O^{18}O$). The

measurement conditions other than pure water containing isotropic water were the same as those in the above-mentioned photocatalytic overall pure-water splitting tests in the smaller vessel.

Results and discussion

Characterization

Figure 1 shows the powder XRD pattern of $ZnRh_2O_4/Ag/Bi_4V_2O_{11}$ after HNO_3 treatment. The XRD peaks mainly correspond to two phases originating from $ZnRh_2O_4$ and $Bi_4V_2O_{11}$ with trace amounts of peaks from some Ag oxide (probably $AgVO_3$). In contrast, no Ag peaks were observed. This is plausible since the amount of Ag remaining in the composite was too small for detection. Thus, most of the Ag was removed by the HNO_3 treatment. The existence of Ag was confirmed and the valency of Ag in the photocatalyst was proved to be mainly zero (Ag^0) by XPS (Figs. S2 and S3 in ESI. 2).

UV-vis absorption spectra of $Bi_4V_2O_{11}$, $ZnRh_2O_4$, and $ZnRh_2O_4/Ag/Bi_4V_2O_{11}$ with and without HNO_3 treatment are shown in Fig. 2. The spectrum for untreated $ZnRh_2O_4/Ag/Bi_4V_2O_{11}$ shows greater absorption than that for the HNO_3-treated $ZnRh_2O_4/Ag/Bi_4V_2O_{11}$ at wavelengths longer than ~600 nm, a property derived from the Ag. After the HNO_3 treatment, the absorption at wavelengths longer than ~600 nm decreased to the same level as that of $ZnRh_2O_4$, resulting in the spectra of $ZnRh_2O_4$ and the HNO_3-treated photocatalyst resembling each other. This is reasonable since the dark brown $ZnRh_2O_4$ powder dominates the brown $Bi_4V_2O_{11}$ powder when the two are mixed. This change in absorption also indicates the removal of Ag from the system.

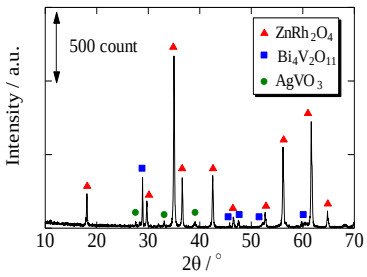

Fig. 1 XRD pattern of $ZnRh_2O_4/Ag/Bi_4V_2O_{11}$ after HNO_3 treatment.

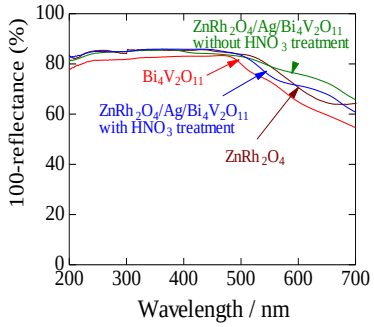

Fig. 2 UV-visible absorption spectra of $Bi_4V_2O_{11}$, $ZnRh_2O_4$, and $ZnRh_2O_4/Ag/Bi_4V_2O_{11}$ (with and without HNO_3 treatment).

Electron microscopy observations

Figure 3 shows a SEM image of the HNO_3-treated $ZnRh_2O_4/Ag/Bi_4V_2O_{11}$ powder. In this image, small $ZnRh_2O_4$ (~200–300 nm) and large $Bi_4V_2O_{11}$ (~10 μm) particles can be clearly observed.

STEM imaging and EDS-based elemental mapping of the HNO_3-treated $ZnRh_2O_4/Ag/Bi_4V_2O_{11}$ were also performed (Figs. 4a–4f, Fig. S4 in ESI. 3 and Fig. S5 in ESI. 4). The $Bi_4V_2O_{11}$ and $ZnRh_2O_4$ particles were distinguishable (Fig. 4a) and were estimated to have sizes of ~4 μm and ~200–300 nm, respectively. The difference in the $Bi_4V_2O_{11}$ particle size estimated from the SEM and STEM images is attributable to the distribution of its particle size which ranges from ~2 to ~10 μm as confirmed using the SEM. Notably, the Ag was clearly distributed (Fig. 4b) between the areas of Zn and Rh (Figs. 4c and 4d) and Bi and V (Figs. 4e and 4f). Although some Ag oxide phase (probably $AgVO_3$) was detected by XRD, the distribution of V did not overlap with that of Ag; thus, we

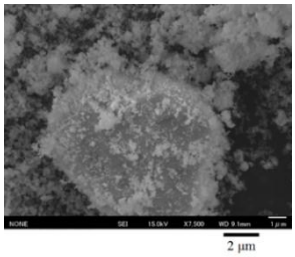

Fig. 3 SEM image of $ZnRh_2O_4/Ag/Bi_4V_2O_{11}$ powder after HNO_3 treatment.

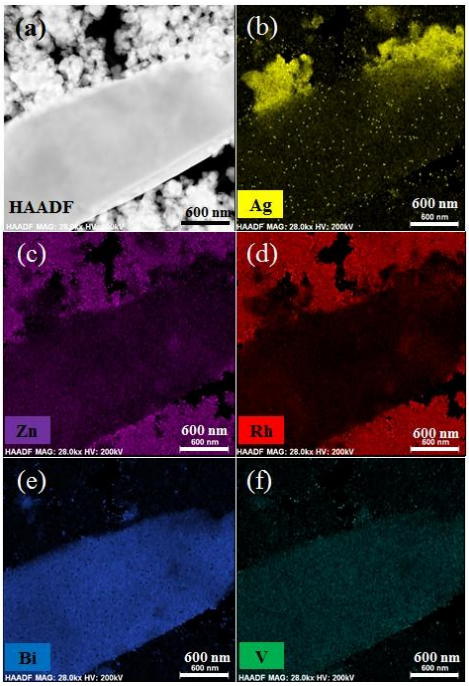

Fig. 4 STEM images of $ZnRh_2O_4/Ag/Bi_4V_2O_{11}$ after HNO_3 treatment. STEM image (a) and EDS element maps (b–f) in which yellow (b), purple (c), red (d), blue (e), and blue-green (f) colors correspond to Ag, Zn, Rh, Bi, and V, respectively.

consider that the Ag was inserted between $ZnRh_2O_4$ and $Bi_4V_2O_{11}$. However, the Ag particle size was unexpectedly larger (200–500 nm, Figs. S2b and S2c) than its size in $ZnRh_2O_4/Ag/Ag_{1-x}SbO_{3-y}$, in which we could not recognize Ag particles.[26] In the case of $ZnRh_2O_4/Ag/Ag_{1-x}SbO_{3-y}$, we performed the heat-treatment at 900°C, slightly below the melting temperature of Ag. In the present study, the heat-treatment temperature was as low as 750°C owing to the limitation imposed by the melting temperature of $Bi_4V_2O_{11}$. Thus, the Ag, the product of the thermal decomposition of Ag_2O at 280°C did not melt and maintained in the form of relatively large particles.

Half water-splitting reaction of $Bi_4V_2O_{11}$

To examine the activity of $Bi_4V_2O_{11}$ as the O_2 evolution photocatalyst, the half reaction of water over $Bi_4V_2O_{11}$ was evaluated using an aqueous solution containing either Ag^+ or Ce^{4+} as the sacrificial agent irradiated with a 610 nm (1.40 mW cm^{-2}) or 700 nm LED (2.43 mW cm^{-2}) lamp (Fig. 5). $Bi_4V_2O_{11}$ was able to produce O_2 under both lamps in the presence of Ce^{4+}. Thus, this photocatalyst was proved to be sensitive to visible light up to a wavelength of at least 700 nm. The AQE value under the 700 nm LED (1.81×10^{-2}%) was smaller than that under the 610 nm LED (5.90×10^{-2}%), which is a typical phenomenon when a photocatalytic reaction proceeds via near-band-edge excitation. In the presence of Ag^+, the O_2 evolution rates were much lower than those in the presence of Ce^{4+} under both LED lamps, and the O_2 evolution rate became negligibly small under the 700 nm LED. This is reasonable when we consider the reduction potentials of Ce^{4+} to Ce^{3+} (1.74 V vs SHE) and Ag^+ to Ag (0.7991 V vs SHE).[28,29] Notably, it can be deduced that the CB bottom potential of $Bi_4V_2O_{11}$ is more negative than 0.7991 V vs SHE, although there should only be a small difference between these potentials.

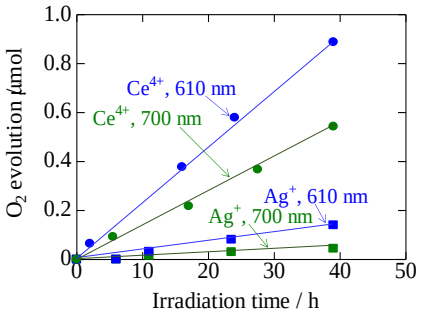

Fig. 5 Photocatalytic O_2 evolution reactions from aqueous $AgNO_3$ solution (squares), aqueous $Ce(SO_4)_2$ solution (circles) over $Bi_4V_2O_{11}$ under irradiation by LED lamp with wavelength of 610 nm (blue) or 700 nm (green).

Typically, the VB tops of Bi oxides, such as $BiVO_4$, are composed of hybrid Bi 6s and O 2p orbitals, and their VB top potentials are similar (~2.5 V vs SHE).[30] By analogy with the fact, the VB top potential of $Bi_4V_2O_{11}$ is presumed to be ~2.5 V. As mentioned above, $Bi_4V_2O_{11}$ was sensitive to visible light up to a wavelength of at least 700 nm, indicating that its Eg is smaller than 1.77 eV. Thus, the CB bottom potential of $Bi_4V_2O_{11}$ is ~0.73 V (vs SHE) or more negative. This coincides with the value estimated from the O_2 evolution in the presence of Ag^+. Note that we have already reported that $ZnRh_2O_4$ can utilize visible light up to a wavelength of at least 770 nm for H_2 evolution.[31] Thus, $ZnRh_2O_4/Ag/Bi_4V_2O_{11}$ is expected to be sensitive to visible light up to at least 700 nm.

Water splitting

Figure 6a shows the time courses of H_2 and O_2 evolution using HNO_3-treated $ZnRh_2O_4/Ag/Bi_4V_2O_{11}$ powders from pure water under irradiation with visible light (>420 nm) and in the dark. In the dark, O_2 was not observed and only a negligible amount of H_2 was observed during the measurement period. In contrast, under visible-light irradiation, an initial induction period of ~10 h was observed, followed by the linear generation of H_2 and O_2 at a molar ratio of 2 to 1. Although the reason for the delay in H_2 and O_2 evolution is unclear, this phenomenon has often been encoutered.[17] It may be due to existing defects, reconstruction of surface states, or the adsorption of H_2 and O_2 molecules on the photocatalyst surface. In the presence of only $Bi_4V_2O_{11}$ in pure water under identical visible light, neither H_2 nor O_2 was detected (Fig. S6 in ESI. 5). It is thermodynamically reasonable that $Bi_4V_2O_{11}$ cannot produce H_2 from water because the CB bottom of $Bi_4V_2O_{11}$ lies at a potential of ~0.73 V (vs SHE). In fact, H_2 could not be detected even in the presence of methanol (Fig. S7 in ESI. 6). Thus, $Bi_4V_2O_{11}$ cannot be the H_2 evolution photocatalyst. In our previous study, we also confirmed that

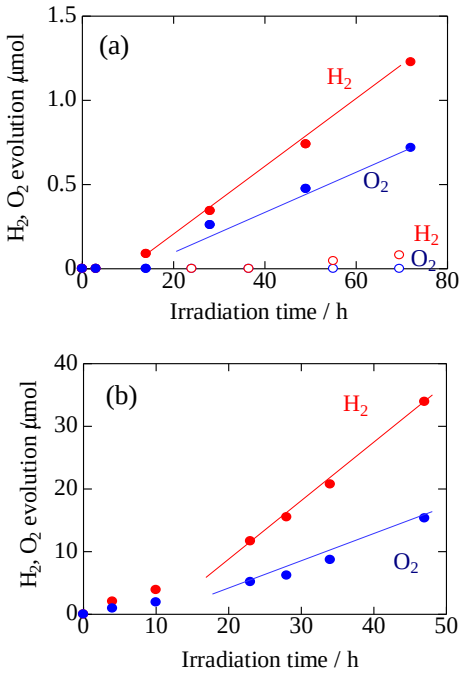

Fig. 6 Time courses of photocatalytic evolution of H_2 (solid red) and O_2 (solid blue) from pure water over $ZnRh_2O_4/Ag/Bi_4V_2O_{11}$ ((a) 60 mg, (b) 600 mg) irradiated with visible light (>420 nm). In (a), the amounts of H_2 and O_2 in the absence of light are also plotted (open red and blue).

$ZnRh_2O_4$ powder cannot produce H_2 or O_2 from pure water.[26] Thus, $Bi_4V_2O_{11}$ and $ZnRh_2O_4$ can generate stoichiometric H_2 and O_2 from pure water only when they are connected to each other with Ag, in which $Bi_4V_2O_{11}$ and $ZnRh_2O_4$ acted as the O_2 and H_2 evolution site, respectively. Next, we attempted to scale up the overall pure-water splitting by increasing the amounts of sample and pure water by a factor of 10 (Fig. 6b). During light irradiation for 40 h, the amounts of H_2 and O_2 evolution were ~25 and ~12 μmol, respectively. Surprisingly, the amounts of H_2 and O_2 evolution were ~40 times as much as those in Fig. 6a, where the amounts of H_2 and O_2 evolution were ~0.6 and ~0.3 μmol, respectively, although the amounts of sample and pure water were increased only tenfold. Although this is a matter for the chemical engineering field, the further improvement of H_2 and O_2 productivity can be expected by optimization of the amounts of photocatalyst and pure water, the shape or volume of the reaction vessel, how the light is irradiated, and so forth.

Water splitting under red-light irradiation

Figures 7a and 7b show the time courses of H_2 and O_2 evolution from pure water (12 mL) over $ZnRh_2O_4/Ag/Bi_4V_2O_{11}$ (60 mg) using 610 nm and 700 nm LED lamps, respectively. The water-splitting tests were performed twice with a newly prepared sample under 610 nm LED light with the same intensity and under 700 nm LED light with different light intensities. The AQE values were calculated from the total number of incident photons from each LED light source and the O_2 evolution rates were calculated from the slopes of the plots (solid and dashed lines) in Fig. 7 (Table 1). For all experiments, after an induction period, H_2 and O_2 evolution rates having a ratio of 2:1 were observed; thus, the obtained AQE values for O_2 evolution were almost the same as those for H_2 evolution. The H_2 and O_2 evolution rates under irradiation with a wavelength of 610 nm were almost the same (naturally, the AQE values were also almost the same), indicating good data reproducibility. In contrast, under irradiation with the 700 nm LED, the H_2 and O_2 evolution rates increased almost linearly with increasing light intensity; thus, the AQE values were nearly identical, regardless of the light intensity. This is reasonable considering that the reaction proceeded under a light-limited condition. Note that this is the first demonstration of $ZnRh_2O_4/Ag/Bi_4V_2O_{11}$ successfully utilizing visible light up to a wavelength of 700 nm (red light) to produce H_2 and O_2 in the stoichiometric ratio.

Table 1 Light intensity, O_2 generation rates, and AQE values in the presence of $ZnRh_2O_4/Ag/Bi_4V_2O_{11}$.

Light source	Light intensity / mW cm^{-2}	O_2 generation rate / μmol h^{-1}	AQE (%)
610 nm LED	1.40	3.89×10^{-3}	1.01×10^{-2}
	1.40	4.31×10^{-3}	1.10×10^{-2}
700 nm LED	2.43	3.18×10^{-3}	4.15×10^{-3}
	4.00	5.36×10^{-3}	4.25×10^{-3}

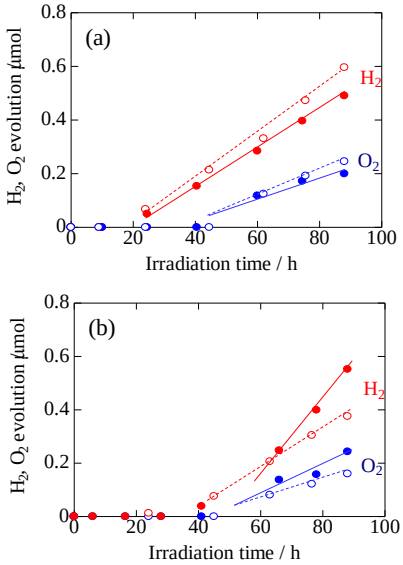

Fig. 7 Time courses of photocatalytic evolution of H_2 (red) and O_2 (blue) from pure water over $ZnRh_2O_4/Ag/Bi_4V_2O_{11}$ irradiated with light of wavelengths (a) 610 nm, (b) 710 nm. Two types of plot (solid and open circles) are shown for 610 nm LED light with the same intensity (a) and for 700 nm LED light with different light intensities (b).

Isotope labeled-water splitting under red-light irradiation

To confirm the liberation of O_2 from water over $ZnRh_2O_4/Ag/Bi_4V_2O_{11}$, we examined water splitting using this system with water containing 33% $H_2{}^{18}O$ under light irradiation with a wavelength of 700 nm (700 nm LED) as shown in Fig. 8.

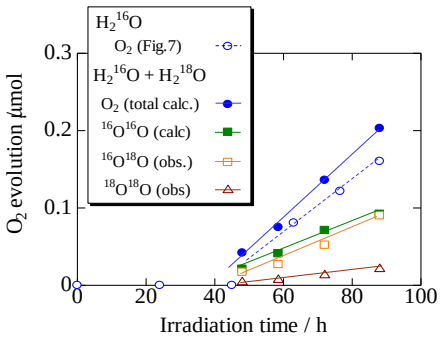

Fig. 8 Results of GCMS spectrometry of splitting for water containing 33% $H_2{}^{18}O$ over $ZnRh_2O_4/Ag/Bi_4V_2O_{11}$ irradiated with the 700 nm LED.

The amount of $^{16}O^{16}O$ (calc. $^{16}O^{16}O$) was obtained using the equation calc. $^{16}O^{16}O$ = obs. $^{16}O^{16}O$ – (obs. $^{14}N^{14}N$ / 0.78) × 0.21 because the detected $^{14}N^{14}N$ (N_2) originated from external air that entered the GCMS system rather than from air dissolved in water according to our previous report.[23,26] If overall water splitting proceeds, the ratio of evolved $^{16}O^{16}O$, $^{16}O^{18}O$, and $^{18}O^{18}O$ should be 4:4:1. In fact, under 700 nm light irradiation for 88 h, $^{16}O^{16}O$, $^{16}O^{18}O$, and $^{18}O^{18}O$ were detected at a ratio of 4.08:3.97:0.946 (Fig. 8 and Table S1 in ESI. 7). In addition, the time course of total O_2 evolution ($^{16}O^{16}O$ + $^{16}O^{18}O$ + $^{18}O^{18}O$) using water containing 33% $H_2{}^{18}O$ was consistent with that using normal $H_2{}^{16}O$ (open blue dots with a broken line in Fig. 8, the same data as in Fig. 7b with the same symbol). Therefore, it was confirmed that O_2 was liberated from water over $ZnRh_2O_4/Ag/Bi_4V_2O_{11}$ under 700 nm light (red light)

irradiation. Combining these results with Fig. 7b and Table 1, we can confidently conclude that the overall pure-water splitting reaction proceeded over the $ZnRh_2O_4/Ag/Bi_4V_2O_{11}$ photocatalyst under visible-light irradiation with a wavelength of 700 nm.

We also examined the pure-water splitting over $ZnRh_2O_4/Bi_4V_2O_{11}$ under visible light (> 420 nm). O_2 was not observed and only a negligible amount of H_2 was observed as shown in Fig. S8 (ESI. 6). In addition, we tested the pure-water splitting by the mixture of $ZnRh_2O_4$, Ag, and $Bi_4V_2O_{11}$ (molar ratio of 6:1:3) irradiated with visible light (> 420 nm). As shown in Fig. S9 (ESI. 6), neither H_2 nor O_2 was observed at all. Thus, we clearly demonstrated that H_2 and O_2 were evolved only when we prepared $ZnRh_2O_4/Ag/Bi_4V_2O_{11}$. Considering our previous report[26] and such findings in the present study that the overall water-splitting reaction does not proceed using $ZnRh_2O_4$ or $Bi_4V_2O_{11}$ alone but is induced over $ZnRh_2O_4/Ag/Bi_4V_2O_{11}$, Ag has an important role in the process. Specifically, Ag acts as a solid-state electron mediator for electron transfer from the CB of $Bi_4V_2O_{11}$ to the VB of $ZnRh_2O_4$. Thus, the photoexcited electrons in $ZnRh_2O_4$ and holes in $Bi_4V_2O_{11}$ can effectively reduce and oxidize water, respectively, producing H_2 and O_2 at a molar ratio of 2:1. Note that the $ZnRh_2O_4/Ag/Bi_4V_2O_{11}$ system is stable under light irradiation up to ~100 h while stirring. This is possibly attributable to the lower calcination temperature of the mixture of $Bi_4V_2O_{11}$, $ZnRh_2O_4$, and Ag at 750°C because polycrystalline $Bi_4V_2O_{11}$ is stable up to 750°C. The increase in the mechanical stability remains unsolved. The band alignments of $ZnRh_2O_4$, Ag, and $Bi_4V_2O_{11}$ and possible charge transfer processes are shown in Scheme S1 in ESI. 8. It is likely that a three-step photoexcitation process is required. The conventional Z-scheme cannot be constructed from a set of H_2 and O_2 photocatalysts, in which the CB bottom potential of the O_2 photocatalyst is more positive than the VB top potential of the H_2 photocatalyst, similar to the set of $ZnRh_2O_4$ and $Bi_4V_2O_{11}$. Thus, the present Ag-inserted heterojunction photocatalyst, where Ag acts as the electron mediator, also has an advantage over the conventional Z-scheme in terms of being able to apply a wide variety of H_2 and O_2 photocatalysts in addition to splitting pure water without any chemicals.

Conclusions

We have established a solid-state Z-scheme for overall pure-water splitting that is sensitive to visible light by inserting Ag between $ZnRh_2O_4$ and $Bi_4V_2O_{11}$. The system simultaneously evolves H_2 and O_2 from pure water at a molar ratio of ~ 2 to 1 under red-light irradiation with a wavelength of 700 nm. In the present study, we used polycrystalline $Bi_4V_2O_{11}$ powder as the O_2 evolution photocatalyst. In contrast, we are now alternating to use $Bi_4V_2O_{11}$ powder obtained by pulverizing single-crystal $Bi_4V_2O_{11}$, with which we will prepare solid-state $ZnRh_2O_4/Ag/Bi_4V_2O_{11}$. Over such a photocatalyst, we can expect an increase in the AQE for overall water splitting. In fact, we have already confirmed an increase in O_2 generation from the half-reaction of water over the single-crystal derivative compared with over the polycrystalline derivative. In addition, we have discovered that single-crystal $Bi_4V_2O_{11}$ is thermally more stable up to 900°C, whereas polycrystalline $Bi_4V_2O_{11}$ is stable up to only 750°C. This allows us to calcine a mixture of $Bi_4V_2O_{11}$, $ZnRh_2O_4$, and Ag at 900°C instead of 750°C, leading to a stronger connection force between Ag and the two types of photocatalyst. Such studies are currently underway in our laboratory.

Acknowledgements

This study was partially supported by the Cooperative Research Program of the Catalysis Research Center, Hokkaido University (Grant #15A1002), and was also supported by CREST, JST.

Notes and references

1 A. Fujishima and K. Honda, *Nature*, 1972, **238**, 37.
2 J. Sato, N. Saito, H. Nishiyama and Y. Inoue, *J. Phys. Chem. B*, 2001, **105**, 6061.
3 K. Domen, A. Kudo, T. Onishi, N. Kosugi and H. Kuroda, *J. Phys. Chem*., 1986, **90**, 292.
4 H. Kato, K. Asakusa and A. Kudo, *J. Am. Chem. Soc*., 2003, **125**, 3082.
5 K. Domen, J. Kondo, M. Hara and T. Takata, *Bull. Chem. Soc. Jpn*., 2000, **73**, 1307.
6 A. Kudo, *Int. J. Hydrogen Energy* 2007, **32**, 2673.
7 K. Maeda, R. Abe and K. Domen, *J. Phys. Chem. Lett*., 2011, **115**, 3057.
8 K. Maeda, K. Teramura, D. Lu, T. Takata, N. Saito, Y. Inoue and K. Domen, *Nature*, 2006, **440**, 295.
9 K. Maeda, T. Takata, M. Hara, N. Saito, Y. Inoue, H. Kobayashi and K. Domen, *J. Am. Chem. Soc*., 2005, **127**, 8286.
10 K. Maeda, K. Teramura, T. Takata, M. Hara, N. Saito, K. Toda, Y. Inoue, H. Kobayashi and K. Domen, *J. Phys. Chem. B*, 2005, **109**, 20504.
11 K. Teramura, K. Maeda, T. Saito, T. Takata, N. Saito, Y. Inoue and K. Domen, *J. Phys. Chem. B*, 2005, **109**, 21915.
12 Y. Lee, H. Terashima, Y. Shimodaira, K. Teramura, M. Hara, H. Kobayashi, K. Domen and M. Yashima, *J. Phys. Chem. C*, 2007, **111**, 1042.
13 H. Liu, J. Yuan, W. Shangguan and Y. Teraoka, *J. Phys. Chem. C*, 2008, **112**, 8521.
14 N. Lei, M. Tanabe and H. Irie, *Chem. Commun.*, 2013, **49**, 10094.
15 P. Dhanasekaran and N. M. Gupta, *Int. J. Hydrogen Ener*., 2012, **37**, 4897.
16 R. Asai, H. Nemoto, Q. Jia, K. Saito, A. Iwase and A. Kudo, *Chem. Commun*., 2014, **50**, 2543.
17 L. Liao, Q. Zhang, Z. Su, Z. Zhao, Y. Wang, Y. Li, X. Lu, D. Wei, G. Feng and Q. Yu et al., *Nat. Nanotechnol.*, 2014, **9**, 69.
18 C. Pan, T. Takata, M. Nakabayashi, T. Matsumoto, N. Shibata, Y. Ikuhara and K. Domen, *Angew. Chem. Int. Ed.*, 2015, **54**, 2955.
19 J. Liu, Y. Liu, N. Liu, Y. Han, X. Zhang, H. Huang, Y. Lifshitz, S. T. Lee, J. Zhong and Z. Kang, *Science*, 2015, **347**, 970.
20 K. Sayama, K. Mukasa, R. Abe, Y. Abe and H. Arakawa, *J. Photochem. Photobiol. A: Chem.*, 2002, **148**, 71.
21 H. Kato, Y. Sasaki, A. Iwase and A. Kudo, *Bull. Chem. Soc. Jpn.*, 2007, **80**, 2457.
22 A. Kudo, *Int. J. Hydrogen Energy*, 2002, **32**, 2673.

23 S. Tanigawa and H. Irie, *Appl. Catal. B: Environ.*, 2016, 180, 1.
24 Y. Sasaki, H. Nemoto, K. Saito, A. Kudo, *J. Phys. Chem. C*, 2009, **113**, 17536.
25 A. Iwase, Y. H. Ng, Y. Ishiguro, A. Kudo and R. Amal, *J. Am. Chem. Soc*., 2011, **133**, 11054.
26 R. Kobayashi, S. Tanigawa, T. Takashima, B. Ohtani and H. Irie, *J. Phys. Chem. C*, 2014, **118**, 22450.
27 V. Thakral and S. Uma, *Mater. Res. Bull.*, 2010, 45, 1250−1254.
28 E. Wadsworth, F. R. Duke and C. A. Goetz, *Anal. Chem.*, 1957, **29**, 1824.
29 A. J. Bard, R. Parsons and J. Jordan, Marcel Dekker, New York, 1985, 294.
30 K. Sayama, A. Nomura, T. Arai, R. Abe, M. Yanagida, T. Oi, Y. Iwasaki, Y. Abe and H. Sugihara, *J. Phys. Chem. B*, 2006, **110**, 11352.
31 Y. Takimoto, T. Kitta and H. Irie, *Inter. J. Hydro. Ener.*, 2012, **37**, 134.